J|A|C|S
ARTICLES

Published on Web 02/03/2010

Effects of Ce^{3+} Codoping and Annealing on Phase Transformation and Luminescence of Eu^{3+}-Doped YPO_4 Nanorods: D_2O Solvent Effect

M. Niraj Luwang,[†] R. S. Ningthoujam,*[,‡] Jagannath ,[§] S. K. Srivastava,[†] and R. K. Vatsa[‡]

Department of Chemistry, Manipur University, Imphal-795003, India, and Chemistry Division and Technical Physics and Prototype Engineering Division, Bhabha Atomic Research Center, Mumbai-400085, India

Received November 11, 2009; E-mail: rsn@barc.gov.in

Abstract: Ce^{3+}- and Eu^{3+}-doped YPO_4 nanorods have been prepared at relatively low temperature (120 °C). A detailed investigation of the role of Ce^{3+} concentration up to 10 atom % on the luminescence intensity of Eu^{3+} in Ce^{3+}- and Eu^{3+}-doped YPO_4 has been carried out. Phase transformation from a tetragonal to a hexagonal structure occurs with increasing Ce^{3+} concentrations, and water molecules are also associated during phase transformation. Thermal study shows that water can be retained up to 800 °C in the hexagonal structure. Interestingly, the hexagonal structure returns to the tetragonal structure on annealing above 900 °C. As-prepared and 500 °C heated samples show uniform sized nanorods, whereas a 900 °C heated sample shows distorted nanorods in which pores are present. Initially, the luminescence intensity decreases sharply with increasing Ce^{3+} concentrations, even for 2 atom %. This is related to the enhanced nonradiative rate as compared to the radiative rate, since multiphonon relaxation to surrounding water molecules increases. This is not due to the possible oxidation−reduction process between Eu^{3+} and Ce^{3+} to give Eu^{2+} and Ce^{4+}, as confirmed by X-ray photoelectron spectroscopy and luminescence studies. Then, a significant enhancement of luminescence intensity occurs on annealing above 900 °C. This can be ascribed to the loss of water molecules during a phase transformation from the hydrated hexagonal to the dehydrated tetragonal phase. To the authors' knowledge, we for the first time performed a luminescent study with a change of solvent from H_2O to D_2O, and significant enhancement in luminescence is found.

1. Introduction

Rare earth ion doped compounds have attracted a great amount of interest, due to their significant technological importance, and are used as high-performance luminescent devices, catalysts, time-resolved fluorescence labels for biological detection, and other functional materials based on their optical, electronic, and chemical characteristics.[1−6] The composition and microstructure of the host play an important role in controlling the chemical, physical, optical, and electronic properties of these rare earth ion doped compounds, and also their properties are strongly affected by the synthetic routes.[7−9] Wet-chemistry synthetic routes, such as sol−gel,[10,11] precipitation,[1,12,13] hydrothermal methods,[8,14] etc. are usually employed, as they provide several adjustable parameters such as pH value, reaction temperature, ripening time, and solution concentration and thereby the size, shape, morphology, and structure of the synthesized materials can be effectively controlled. Especially in the synthesis of rare earth doped compounds, the doped ions get uniformly dispersed in the crystal lattice of the host,[15,16] and this gives rise to the enhanced

[†] Manipur University.
[‡] Chemistry Division, Bhabha Atomic Research Center.
[§] Technical Physics and Prototype Engineering Division, Bhabha Atomic Research Center.

(1) Riwotzki, K.; Meyssamy, H.; Schnablegger, H.; Kornowski, A.; Haase, M. H. *Angew. Chem., Int. Ed.* **2001**, *40*, 573.
(2) Nishihama, S.; Hirai, T.; Komasawa, I. *J. Mater. Chem.* **2002**, *12*, 1053.
(3) Fang, Z. M.; Hong, Q.; Zhou, Z. H.; Dai, S. J.; Weng, W. Z.; Wan, H. L. *Catal. Lett.* **1999**, *61*, 39.
(4) Levine, A. K.; Palilla, F. C. *Appl. Phys. Lett.* **1964**, *5*, 118.
(5) Davis, J. B.; Marshal, D. B.; Morgan, P. E. D. *J. Eur. Ceram. Soc.* **2000**, *20*, 583.
(6) Ningthoujam, R. S.; Sudarsan, V.; Godbole, S. V.; Tyagi, A. K.; Kienle, L.; Kulshreshtha, S. K. *Appl. Phys. Lett.* **2007**, *90*, 173113.
(7) Yamaguchi, T.; Ishii, N.; Tashiro, K.; Aida, T. *J. Am. Chem. Soc.* **2003**, *125*, 13934.
(8) Fang, Y. P.; Xu, A. W.; Song, R. Q.; Zhang, H. X.; You, L. P.; Yu, J. C.; Liu, H. Q. *J. Am. Chem. Soc.* **2003**, *125*, 16025.
(9) Song, H. W.; Yu, L. X.; Lu, S. Z.; Wang, T.; Liu, Z. X.; Yang, L. M. *Appl. Phys. Lett.* **2004**, *85*, 470.
(10) Rajesh, K.; Mukundan, P.; Krishna Pillai, P.; Nair, V. R.; Warrier, K. G. K. *Chem. Mater.* **2004**, *16*, 2700.
(11) Nedelec, J. M.; Mansuy, C.; Mahiou, R. *J. Mol. Struct.* **2003**, *651−653*, 165.
(12) Riwotzki, K.; Meyssamy, H.; Kornowski, A.; Haase, M. *J. Phys. Chem., B* **2000**, *104*, 2824.
(13) Ningthoujam, R. S.; Shukla, R.; Vatsa, R. K.; Duppel, V.; Kienle, L.; Tyagi, A. K. *J. Appl. Phys.* **2009**, *105*, 084304.
(14) Meyssamy, H.; Riwotzki, K.; Kornowski, A.; Naused, S.; Haase, M. *Adv. Mater.* **1999**, *11*, 840.
(15) Singh, L. R.; Ningthoujam, R. S.; Sudarsan, V.; Srivastava, I.; Singh, S. D.; Dey, G. K.; Kulshreshtha, S. K. *Nanotechnology* **2008**, *19*, 055201.
(16) Singh, N. S.; Ningthoujam, R. S.; Devi, L. R.; Yaiphaba, N.; Sudarsan, V.; Singh, S. D.; Vatsa, R. K.; Tewari, R. *J. Appl. Phys.* **2008**, *104*, 104307.

 © 2010 American Chemical Society

luminescent intensity. However, in the wet-chemistry synthesis of inorganic luminescent materials, luminescent quenchers such as OH^-, CO_3^{2-}, etc. can be adsorbed on the material surface and be coordinated with the rare-earth ions.[17,18] Usually OH^- ions with high vibrational frequency provide an efficient means to quench the luminescence of rare-earth ions.[17] Di et al.[19] have reported the abnormal behavior of luminescence on increasing crystallinity. With increasing crystallinity of monoclinic phase Tb-doped yttrium orthophosphate, the luminescence intensity decreases. They explained this behavior on the basis of the content of water molecules. During crystallinity, water molecules increase and thereby the nonradiative rate increases with an increase of water molecules.[19] However, in most cases, it was found to be opposite.

In wet-chemical synthesis, control of water molecules associated in any phase structure is difficult. Even the hexagonal structure of lanthanide phosphate is stabilized by water molecules.[21] There are many reports on Ce- and Tb-doped Y/Gd/$LaPO_4$ where enhancement of luminescence of Tb^{3+} occurs with codoping with Ce^{3+}.[22,23] This is attributed to energy transfer from Ce^{3+} to Tb^{3+}.

Could this enhancement happen in Ce^{3+}-codoped YPO_4:Eu? The role of Ce^{3+} concentration in the luminescence and phase transformation of YPO_4:Eu has not been studied much. There are also not many studies regarding the luminescence recovery of these materials doped with rare-earth ions, quenched by the presence of a luminescence quencher such as OH^- ions.

In this study, we have prepared Eu^{3+}-doped YPO_4 (YPO_4:Eu) and Ce^{3+}-codoped YPO_4:Eu at a relatively low temperature of 120 °C for 2 h using a polyethylene glycol−glycerol mixture, which acts as a capping agent. The correlation among phase transformation, content of water molecules, and luminescence intensity of Eu^{3+} has been studied using X-ray diffraction (XRD), in situ high temperature XRD, infrared spectroscopy (IR), thermogravimetric-mass spectroscopy (TG-MS), transmission electron microscopy (TEM), X-ray photoelectron spectroscopy (XPS), and luminescence techniques. Two important results are found: (i) a phase transformation from a tetragonal to a hexagonal structure on increasing Ce^{3+} concentrations in YPO_4:Eu and then reversion to a tetragonal structure on annealing above 900 °C and (ii) a steep decrease in the luminescence intensity of Eu^{3+} with increasing Ce^{3+} concentrations and then a sudden increase in luminescence intensity of Eu^{3+} on annealing the sample above 900 °C.

We performed luminescence measurements of these samples with a change of solvent from H_2O to D_2O. Significant enhancement in luminescence is observed for the first time in these samples.

2. Results and Discussion

2.1. XRD Study. Figure 1 shows the X-ray diffraction (XRD) patterns of as-synthesized pure YPO_4, $Eu_{0.05}Y_{0.95}PO_4$, and

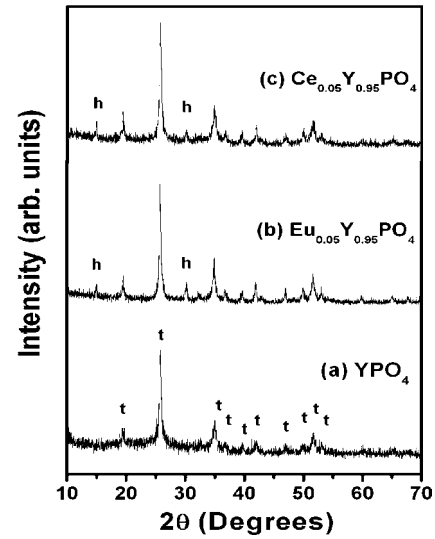

Figure 1. XRD patterns of (a) pure YPO_4, (b) $Eu_{0.05}Y_{0.95}PO_4$, and (c) $Ce_{0.05}Y_{0.95}PO_4$.

$Ce_{0.05}Y_{0.95}PO_4$. As-synthesized pure YPO_4 is a well-crystalline tetragonal phase (JCPDS card no. 11-0254). $Eu_{0.05}Y_{0.95}PO_4$ or $Ce_{0.05}Y_{0.95}PO_4$ shows a well crystalline tetragonal system (denoted by the symbol "t", which stands for tetragonal), and extra diffraction peaks (denoted by the symbol "h" for the hexagonal phase) are also observed. However, these extra peaks are weak as compared to those of the tetragonal phase. These extra peaks are due to the presence of the hexagonal phase in the tetragonal phase. Eu^{3+} or Ce^{3+} ion doping to YPO_4 introduces a hexagonal phase in addition to a prominent tetragonal phase. On the basis of a tetragonal structure, the lattice parameters of pure YPO_4 are $a = 6.897$ Å and $c = 6.037$ Å. The lattice parameters, unit cell volume, and crystallite size calculated for all of the samples are summarized in Table 1 along with the reported values of YPO_4 (JCPDS card no. 11-0254) and hydrated YPO_4 (JCPDS card no. 42-0082). The unit cell volume increases slightly with Eu^{3+} or Ce^{3+} doping in YPO_4. This suggests the substitution of Y^{3+} (1.01 Å) ion by Eu^{3+} (1.07 Å) or Ce^{3+} (1.14 Å). The hexagonal phase contains water in hydrated form as $A_{0.05}Y_{0.95}PO_4 \cdot xH_2O$ (A = Eu, Ce) ($YPO_4 \cdot 0.08H_2O$, JCPDS card no. 42-0082).

Figure 2 shows the XRD patterns of $Ce_xEu_{0.05}Y_{0.95-x}PO_4$ ($x = 0.02, 0.05, 0.07, 0.10$). A mixture of hexagonal and tetragonal phases is obtained. At $x = 0.10$, the amount of tetragonal phase is almost negligible, and only hexagonal phase is observed. With an increase in the Ce^{3+} content, the formation of a hexagonal phase is found.

As-synthesized $Ce_{0.10}Eu_{0.05}Y_{0.85}PO_4$ was annealed at different temperatures to check the stability of the hexagonal phase (hydrated), and we found out that it is stable up to 800 °C. As the annealing temperature is increased to 900 °C, the hydrated hexagonal phase transforms to a dehydrated tetragonal phase, as shown in Figure 3. The above results indicate that the hexagonal phase (hydrated) is stable up to a very high temperature (800 °C) when doped with Eu^{3+} and Ce^{3+}. Earlier reports[21,24] have shown the phase transformation from a hydrated hexagonal phase to a dehydrated monoclinic phase in the temperature range of 200−230 °C. Zollfrank et al.[25] also

(17) Mass, H.; Currao, A.; Calzaferri, G. *Angew. Chem., Int. Ed.* **2002**, *41*, 2495.
(18) Jiang, X. C.; Yan, C. H.; Sun, L. D.; Wei, Z. G.; Liao, C. S. *J. Solid State Chem.* **2003**, *175*, 245.
(19) Di, W.; Wang, X.; Chen, B.; Lu, S.; Ren, X. *Appl. Phys. Lett.* **2006**, *88*, 011907.
(20) Mooney, R. C. L. *J. Chem. Phys.* **1948**, *16*, 1003.
(21) Di, W.; Wang, X.; Chen, B.; Lu, S.; Zhao, X. *J. Phys. Chem. B* **2005**, *109*, 13154.
(22) Li, Q.; Yam, V. W. W. *Angew. Chem., Int. Ed.* **2007**, *46*, 3486.
(23) Buhler, G.; Feldmann, C. *Angew. Chem., Int. Ed.* **2006**, *45*, 4864.
(24) Di, W.; Wang, X.; Chen, B.; Lu, S. *Mater. Lett.* **2005**, *59*, 2310.
(25) Zollfrank, C.; Scheel, H.; Brungs, S.; Greil, P. *Cryst. Growth Des.* **2008**, *6*, 776.

Table 1. Lattice Parameters, Unit Cell Volumes, and Crystallite Size of $Ce_xEu_yY_{1-x-y}PO_4$ ($x = 0.00, 0.02, 0.05, 0.07, 0.10$, $y = 0.05$) at Different Annealing Temperatures along with JCPDS Card Nos. 11-0254 and 42-0082

sample no.	sample	lattice params (Å)		unit cell vol V (Å^3)	crystallite size (nm)
		a	c		
1	YPO_4 (tetragonal, t) JCPDS card no. 11-0254	6.904	6.035	287.66	
2	$YPO_4 \cdot 0.8H_2O$ (hexagonal, h) JCPDS card no. 42-0082	6.833	6.291	254.37	
3	pure YPO_4, as prepared (t)	6.897	6.037	287.20	21.1
4	pure YPO_4, 900 °C (t)	6.895	6.019	286.19	30.0
5	$Eu_{0.05}Y_{0.95}PO_4$, as prepared (t)	6.911	6.036	288.24	25.0
6	$Ce_{0.05}Y_{0.95}PO_4$, as prepared (t)	6.906	6.041	288.10	20.7
7	$Ce_{0.02}Eu_{0.05}Y_{0.93}PO_4$, as prepared (t)	6.911	6.049	288.93	17.7
8	$Ce_{0.05}Eu_{0.05}Y_{0.90}PO_4$, as prepared (h)	6.838	6.288	254.60	23.8
9	$Ce_{0.07}Eu_{0.05}Y_{0.88}PO_4$, as prepared (h)	6.845	6.302	255.73	30.2
10	$Ce_{0.10}Eu_{0.05}Y_{0.85}PO_4$, as prepared (h)	6.853	6.294	255.99	31.8
11	$Ce_{0.10}Eu_{0.05}Y_{0.85}PO_4$, 300 °C (h)	6.848	6.306	256.05	27.4
12	$Ce_{0.10}Eu_{0.05}Y_{0.85}PO_4$, 500 °C (h)	6.844	6.292	255.24	29.1
13	$Ce_{0.10}Eu_{0.05}Y_{0.85}PO_4$, 700 °C (h)	6.848	6.296	255.68	29.8
14	$Ce_{0.10}Eu_{0.05}Y_{0.85}PO_4$, 800 °C (h)	6.843	6.303	255.59	27.7
15	$Ce_{0.10}Eu_{0.05}Y_{0.85}PO_4$, 900 °C (t)	6.910	6.034	288.15	37.1

reported a phase transformation from hydrated europium(III) orthophosphate, $EuPO_4 \cdot nH_2O$, of hexagonal crystal structure to monoclinic non-hydrated $EuPO_4$ at 600 °C.

In situ high-temperature XRD studies of the $Ce_{0.10}Eu_{0.05}Y_{0.85}PO_4$ sample were analyzed at different temperatures from 500 to 1000 °C (Figure 4). In order to make sure that all the hydrocarbon from the sample is removed, as-synthesized $Ce_{0.10}Eu_{0.05}Y_{0.85}PO_4$ was preheated at 500 °C before recording the data. As the annealing temperature increased, a hexagonal phase was observed up to 800 °C and phase transitions to the tetragonal phase occurred at 900 °C. The tetragonal phase remains stable even after cooling at room temperature after heating at 1000 °C. Lattice expansion is observed in both phases on annealing at higher temperature (up to 1000 °C), and then lattice contraction occurs on cooling to room temperature. This is summarized in Table 2.

2.2. TGA and DTA Studies. The thermal properties of $Ce_{0.10}Eu_{0.05}Y_{0.85}PO_4$ were investigated by thermogravimetric analysis (TGA) and differential thermal analysis (DTA), as shown in Figure 5a. The initial weight loss of 4% in the TGA curve below 200 °C, accompanied by an endothermic peak at 188 °C, is assigned to the loss of free water molecules present in the sample.[26] The exothermic peak centered at 280 °C in the DTA curve and the change of weight (3%) in the temperature range of 200−400 °C in the TGA curve is due to the loss of the capping agent, PEG and glycerol.[27] The sharp exothermic peak at 915 °C is assigned to the crystal structure transformation from the hexagonal phase (hydrated) to the tetragonal phase (dehydrated). This transition at 915 °C is confirmed by an in situ high-temperature XRD study (Figure 4), which shows a small amount of the hexagonal phase for the 900 °C sample. The slight difference in phase transition is due to the difference in the duration of annealing at particular temperature. It should be noted that the apparent increase in weight (TGA curve) above 600 °C is due to an artifact.

Thermogravimetric analysis−mass spectrometry (TGA-MS) was utilized to study the evolution of particular gas species with changes in temperature. The TG-DTA curve of $Ce_{0.10}Eu_{0.05}Y_{0.85}PO_4$ is shown in Figure S1 (see the Supporting Information). The features of TGA-MS are similar to those of the normal TGA-DTA curve (Figure 5a). Figure 5b represents

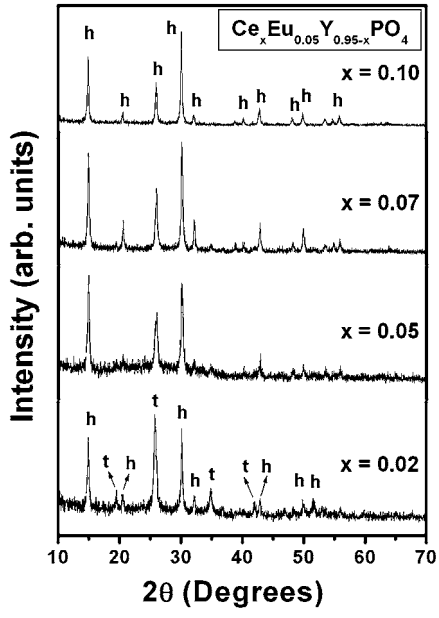

Figure 2. XRD patterns of $Ce_xEu_{0.05}Y_{0.95-x}PO_4$ ($x = 0.02, 0.05, 0.07, 0.10$).

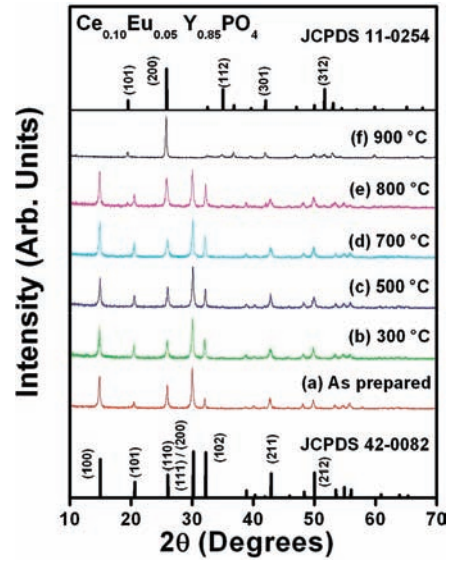

Figure 3. XRD patterns of $Ce_{0.10}Eu_{0.05}Y_{0.85}PO_4$ at different annealing temperatures (a−f) along with the JCPDS card nos. 42-0082 and 11-0254.

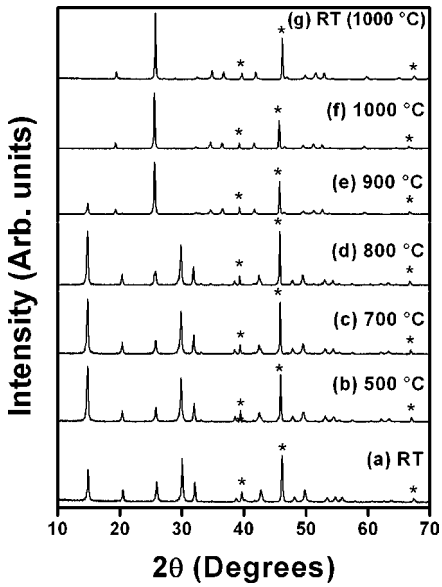

Figure 4. In situ XRD patterns of 500 °C preheated $Ce_{0.10}Eu_{0.05}Y_{0.85}PO_4$ at different temperatures. RT indicates room temperature, and RT (1000 °C) indicates room temperature after cooling from 1000 °C. Asterisks indicate the XRD peaks of Pt, which is used as a sample holder.

Table 2. Lattice Parameters and Unit Cell Volumes of $Ce_{0.10}Eu_{0.05}Y_{0.85}PO_4$ at Different Annealing Temperatures for in Situ XRD along with JCPDS Card Nos. 11-0254 and 42-0082

sample no.	sample	lattice params (Å) a	lattice params (Å) c	unit cell vol V (Å^3)	crystallite size (nm)
1	YPO_4 (tetragonal, t) JCPDS card no. 11-0254	6.904	6.035	287.66	
2	$YPO_4 \cdot 0.8H_2O$ (hexagonal, h) JCPDS card no. 42-0082	6.833	6.291	254.37	
3	$Ce_{0.10}Eu_{0.05}Y_{0.85}PO_4$, 500 °C room temp (h)	6.853	6.293	255.92	30.8
4	500 °C (h)	6.918	6.297	260.98	29.8
5	700 °C (h)	6.932	6.281	261.37	30.0
6	800 °C (h)	6.928	6.307	262.19	31.3
7	900 °C (t)	6.948	6.092	294.10	37.8
8	1000 °C (t)	6.979	6.054	294.85	43.6
9	room temp−cooling (t)	6.908	6.045	288.43	45.9

the prominent gas evolutions, such as water and carbon dioxide, at particular temperatures.

2.3. IR Study. Figure 6 shows infrared (IR) absorption spectra of as-synthesized pure YPO_4, $Eu_{0.05}Y_{0.95}PO_4$, $Ce_{0.05}Y_{0.95}PO_4$, $Ce_{0.10}Eu_{0.05}Y_{0.85}PO_4$, and 900 °C heated $Ce_{0.10}Eu0_{.05}Y_{0.85}PO_4$. The IR spectra of all the analyzed samples show the typical peaks of $(PO_4)^{3-}$ at 526 and 647 cm^{-1}, attributed to bending vibrations commonly known as the ν_4 region,[28,29] and strong bands centered at 1110 and 1077 cm^{-1} merged together, corresponding to stretching vibrations generally known as the ν_3 region.[28,29] Peaks at 1634 and 3442 cm^{-1} correspond to bending and stretching vibrations, respectively, for the O−H group of the PEG−glycerol mixture, which is used as a capping agent for nanoparticles or water associated in the particles.[30] Bonding vibrations of Y−O, Ce−O, or Eu−O occur in the

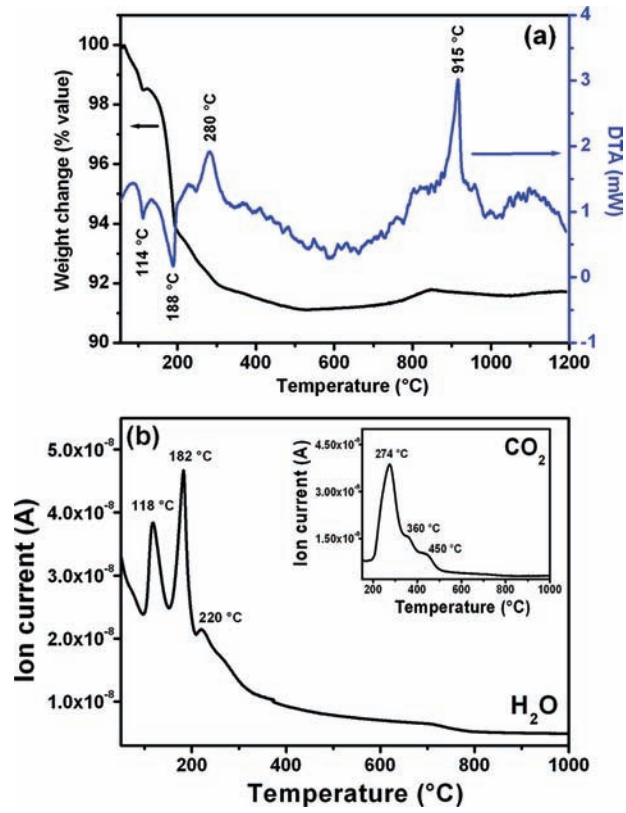

Figure 5. (a) Thermogravimetric analysis (TGA) and differential thermal analysis (DTA) of $Ce_{0.10}Eu_{0.05}Y_{0.85}PO_4$ nanorods and (b) thermogravimetric mass spectrometry analysis (TG-MS) of H_2O and CO_2 in $Ce_{0.10}Eu_{0.05}Y_{0.85}PO_4$ nanorods.

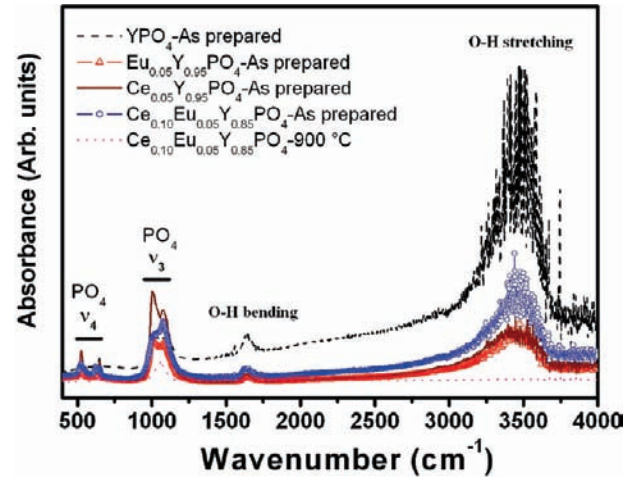

Figure 6. IR absorption spectra of as-prepared samples of (a) YPO_4, (b) $Eu_{0.05}Y_{0.95}PO_4$, (c) $Ce_{0.05}Y_{0.95}PO_4$, and (d) $Ce_{0.10}Eu_{0.05}Y_{0.85}PO_4$ and (e) a 900 °C heated sample of $Ce_{0.10}Eu_{0.05}Y_{0.85}PO_4$.

region 500−550 cm^{-1}. However, these bands are merged with PO_4^{3-} vibrations. Stretching vibrations of CH_2 groups present in PEG−glycerol are observed at ∼2900 cm^{-1}, but their intensity is very weak. The loss of the O−H vibration in the 900 °C heated $Ce_{0.10}Eu_{0.05}Y_{0.85}PO_4$ further confirms the transition from a hexagonal hydrated to a tetragonal dehydrated phase.

2.4. TEM Study. Figure 7 shows the transmission electron microscopy (TEM) images of the as-prepared $Ce_{0.10}Eu_{0.05}Y_{0.85}PO_4$

(26) Yan, R.; Sun, X.; Wang, X.; Peng, Q.; Li, Y. *Chem. Eur. J.* **2005**, *11*, 2183.
(27) Grandi, S.; Magistris, A.; Mustarelli, P.; Quartarone, E.; Tomasi, C.; Meda, L. *J. Non-Cryst. Solids* **2006**, *352*, 273.
(28) Kemp, W. *Organic Spectroscopy*; Macmillan: Hampshire, U.K., 1975.
(29) Begun, G. M.; Beall, G. W.; Boatner, L. A.; Gregor, W. J. *J. Raman Spectrosc.* **1981**, *11*, 273.
(30) Nakamoto, K., *Infrared and Raman Spectra of Inorganic and Coordination Compounds*; Wiley: New York, 1986.

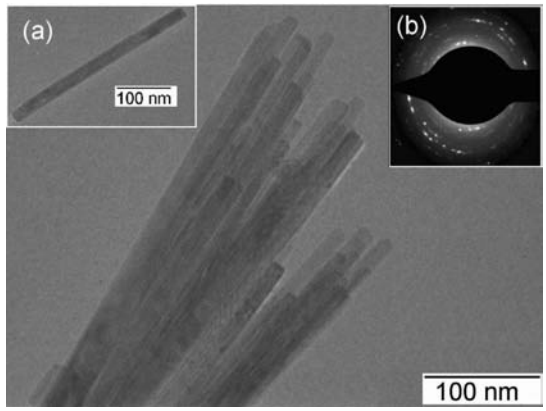

Figure 7. TEM image of as-prepared $Ce_{0.10}Eu_{0.05}Y_{0.85}PO_4$. Insets: (a) a single nanorod; (b) its SAED.

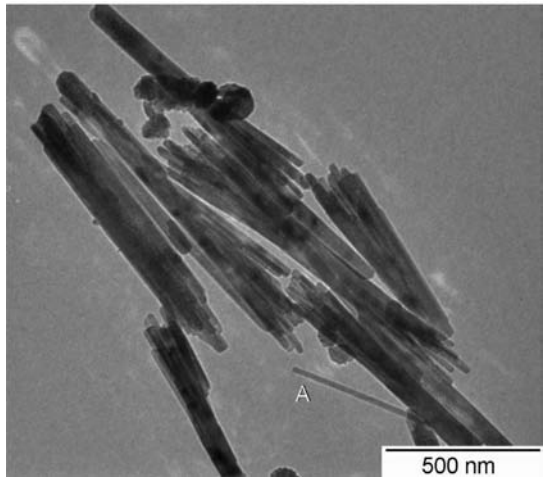

Figure 8. TEM image of 500 °C heated $Ce_{0.10}Eu_{0.05}Y_{0.85}PO_4$. The letter "A" indicates an individual nanorod.

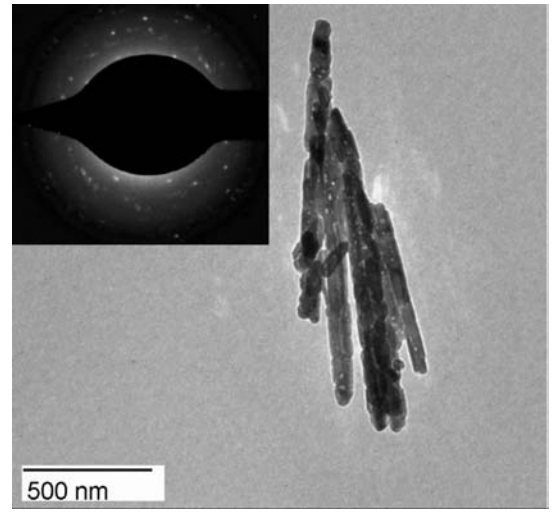

Figure 9. TEM image of 900 °C heated $Ce_{0.10}Eu_{0.05}Y_{0.85}PO_4$ along with its SAED (inset).

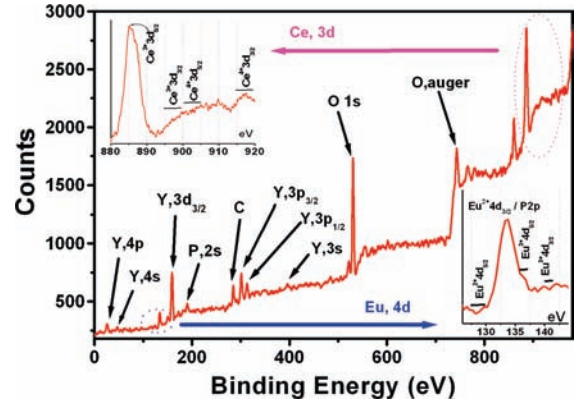

Figure 10. XPS spectra of as-prepared $Ce_{0.02}Eu_{0.05}Y_{0.93}PO_4$. Insets: (upper left) Ce 3d; (lower right) Eu 4d and P 2p.

sample. Nanorods having a diameter of 20 nm and a length of 0.4−1 μm are seen. A single nanorod of 20 nm diameter and 400 nm length is shown in inset a of Figure 7. Its apical ratio is found to be 20. Inset b of Figure 7 shows the selected area electron diffraction (SAED) image of the sample, which represents a well-crystalline sample. The 500 °C heated sample forms nanorods 20−30 nm in diameter and 0.5−1 μm in length (Figure 8). An individual nanorod marked "A" in Figure 8 is 20 nm in diameter and 500 nm in length. It is observed that, with heat treatment up to 500 °C, the morphology of particles does not change much. When the annealing temperature is increased to 900 °C, the nanorods become distorted and break up into smaller particles as can be seen in Figure 9. Numbers of pores or holes could also be observed in the distorted nanorods. SAED study (Figure 9 inset) shows that the sample is well crystalline. The possible reason for the distortion of nanorods as well as the emergence of pore or holes could be due to the void left by the loss of water molecules when the hexagonal hydrated phase changes to the tetragonal dehydrated phase as discussed earlier.

2.5. XPS Study. As-prepared $Ce_{0.02}Eu_{0.05}Y_{0.93}PO_4$ has been analyzed by X-ray photoelectron spectroscopy (XPS) in the range of 0−1000 eV as shown in Figure 10. XPS peaks corresponding to different levels of cerium, europium, yttrium, phosphorus, and oxygen are observed. A strong peak is seen at around 885 eV, which is assigned to Ce^{3+} $3d_{5/2}$,[31,32] but no peaks corresponding to Ce^{4+} 3d are observed at its expected region, as shown in Figure 10 (inset upper left). In Figure 10 (inset lower right), an intense peak centered around 133.7 eV (Eu^{2+} $4d_{3/2}$) with a shoulder at 135 eV (Eu^{3+} $4d_{5/2}$) for all the analyzed samples is observed. Figure 11 shows the XPS spectra of cerium and europium for as-prepared and 900 °C heated samples of $Ce_{0.02}Eu_{0.05}Y_{0.93}PO_4$ and $Ce_{0.10}Eu_{0.05}Y_{0.85}PO_4$. Interestingly, no peak at 128 eV which is particular for Eu^{2+} $4d_{5/2}$ but a small hump at 141 eV corresponding to Eu^{3+} $4d_{5/2}$ is observed. The peak at 133.7 eV might be due to the P 2p, which also appears in this region in the phosphate group.[32,33] XPS analysis confirms that there is no charge exchange between Eu^{3+} and Ce^{3+}, as peaks corresponding to Eu^{2+} and Ce^{4+} are not observed. In the photoluminescence studies (discussed later), Eu^{2+} emission is not observed on excitation at 255 nm (Eu−O charge transfer). Table 3 summarizes all the corresponding values of binding energy of Ce, Eu, Y, P, and O. XPS spectra of 900 °C heated $Ce_{0.02}Eu_{0.05}Y_{0.93}PO_4$ and as-prepared and 900 °C heated

(31) Vercaemst, R.; Poelman, D.; Van Meirhaeghe, R. L.; Fiermans, L.; Laflere, W. H.; Cardon, F. *J. Lumin.* **1995**, *63*, 19.
(32) Wagner, C. D.; Muilenberg, G. E. et al. *Handbook of X-ray Photoelectron Spectroscopy*; Perkin-Elmer: Eden, Prairie, MN, 1979.
(33) Mabiala, J. M. P.; Lenzi, M.; Lenji, J.; Lebugle, A. *Surf. Interface Anal.* **1990**, *15*, 663.

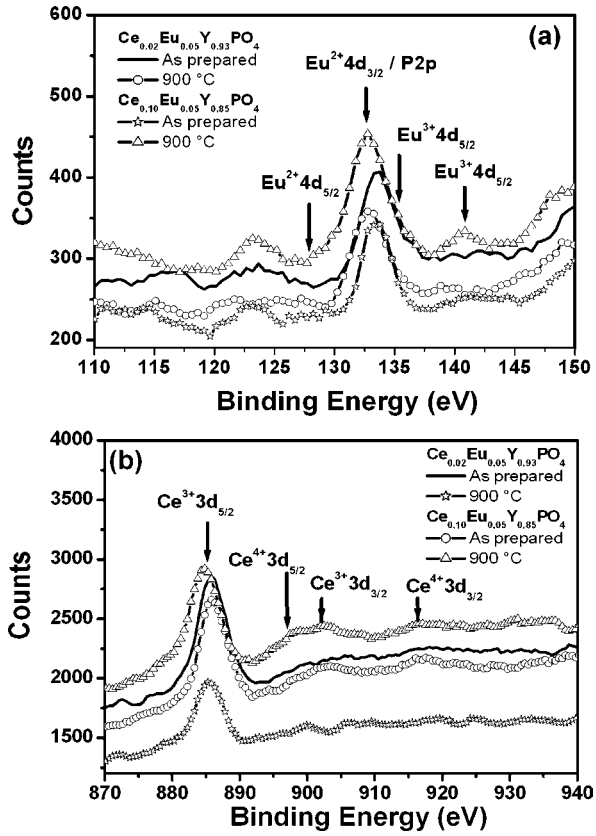

Figure 11. XPS spectra of (a) Eu 4d and (b) Ce 3d for $Ce_{0.02}Eu_{0.05}Y_{0.93}PO_4$ and $Ce_{0.10}Eu_{0.05}Y_{0.85}PO_4$ (as prepared and 900 °C).

Table 3. Binding Energy Values of Eu, Ce, Y, P, and O in $Ce_xEu_yY_{1-x-y}PO_4$ Nanoparticles, As-Prepared and Annealed at 900 °C[a]

		$Ce_{0.02}Eu_{0.05}Y_{0.93}PO_4$		$Ce_{0.10}Eu_{0.05}Y_{0.85}PO_4$	
system		as prepared	900 °C	as prepared	900 °C
Eu^{2+}	$4d_{5/2}$		127.8 (vw)	128.9 (vw)	
	$4d_{3/2}$	133.7 (w)	133.5 (w)	133.3 (w)	133.3 (w)
Eu^{3+}	$4d_{5/2}$	136.1 (vw)	136.0 (vw)	135.5 (vw)	136.4 (vw)
	$4d_{3/2}$	139.7 (vw)	139.5 (vw)	141.1 (b)	141.3 (w)
Ce^{3+}	$3d_{5/2}$	885.1 (vs)	885.4 (vs)	884.5 (vs)	885.1 (vs)
	$3d_{3/2}$				900.0 (vw)
Ce^{4+}	$3d_{5/2}$				
	$3d_{3/2}$	917.3 (vw)	916.8 (vw)	917.0 (vw)	918.7 (vw)
Y	4p	25.8 (w)	25.3 (w)	26.6 (w)	25.7 (w)
	4s	47.0 (vw)	46.9 (vw)	46.3 (vw)	46.9 (vw)
	$3d_{3/2}$	158.5 (s)	159.3 (s)	158.8 (s)	158.5 (s)
	$3p_{3/2}$	300.8 (s)	301.2 (s)	301.1 (s)	300.9 (s)
	$3d_{1/2}$	312.9 (w)	312.8 (w)	312.7 (w)	312.5 (w)
	3s	395.2 (vw)	396.4 (vw)	394.5 (vw)	394.3 (vw)
P	2p	133.7 (w)	133.5 (w)	133.6 (w)	133.3 (w)
	2s	190.3 (w)	191.0 (w)	190.6 (w)	190.3 (w)
O	1s	530.5 (vs)	530.6 (vs)	530.2 (vs)	529.9 (vs)

[a] The labels vw, w, s, vs, and b indicates very weak, weak, sharp, very sharp, and broad, respectively.

$Ce_{0.10}Eu_{0.05}Y_{0.85}PO_4$ are shown in Figures S2−S4, respectively (see the Supporting Information).

2.6. BET Surface Area Study. From the BET surface area analysis, the specific surface areas (A_{sp}) are found to be 19.0 and 60.2 m^2/g, respectively, for as-prepared and 900 °C heated $Ce_{0.10}Eu_{0.05}Y_{0.85}PO_4$. The densities ($D_e$) calculated from the XRD data for as-prepared (hexagonal) and 900 °C heated (tetragonal) $Ce_{0.10}Eu_{0.05}Y_{0.85}PO_4$ are 3.7 and 4.3 g/cm^3, respectively. The density of the sample was calculated, keeping in mind that for

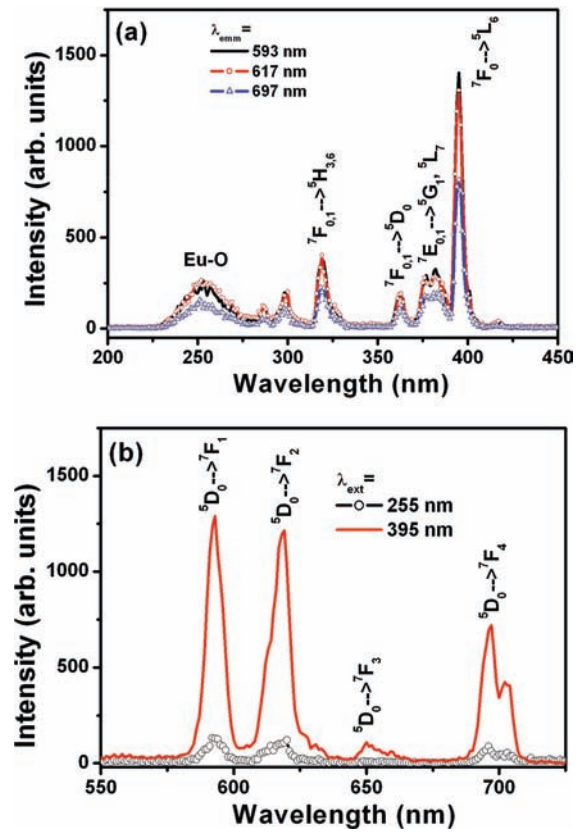

Figure 12. (a) Excitation and (b) emission spectra of $Eu_{0.05}Y_{0.95}PO_4$.

YPO_4 three molecules constitute a hexagonal unit cell volume and four molecules constitute a tetragonal unit cell volume. The particle size (d) is calculated using the equation

$$d = \frac{6}{A_{sp}D_e} \quad (1)$$

As-prepared and 900 °C heated $Ce_{0.10}Eu_{0.05}Y_{0.85}PO_4$ have particle sizes of 85 and 23 nm, respectively.

2.7. Photoluminescence Study. 2.7.1. Excitation and Emission Studies. Figure 12a shows the excitation spectra of as-prepared $Eu_{0.05}Y_{0.95}PO_4$ nanoparticles by monitoring emissions at 593, 617, and 697 nm. A broad peak centered at 255 nm is observed, which is attributed to the Eu−O charge transfer band (CTB). This arises from the transition of 2p electrons of O^{2-} to the empty 4f orbitals of Eu^{3+} ions.[34−36] In addition, peaks at 318, 362, 376/381, and 395 nm were also observed which correspond to $^7F_{0,1}\rightarrow{}^5H_{3,6}$, $^7F_{0,1}\rightarrow{}^5D_0$, $^7F_{0,1}\rightarrow{}^5G_1$,$^5L_7$, and $^7F_0\rightarrow{}^5L_6$ transitions of Eu^{3+}, respectively.[8,37]

Figure 12b shows the emission spectra of as-prepared $Eu_{0.05}Y_{0.95}PO_4$ nanoparticles when excited at wavelengths of 255 and 395 nm. The spectra exhibit a typical emission peak of Eu^{3+} at 593 nm corresponding to the magnetic dipole transition $^5D_0\rightarrow{}^7F_1$ along with peaks at 618 and 697 nm corresponding to the electric dipole transitions $^5D_0\rightarrow{}^7F_2$ and $^5D_0\rightarrow{}^7F_4$, respectively.[8] Apart from these, a weak emission peak centered at

(34) Yu, L.; Li, D.; Yue, M.; Yao, J.; Lu, S. *Chem. Phys.* **2006**, *326*, 478.
(35) Yu, L.; Song, H.; Lu, S.; Liu, Z.; Yang, L.; Kong, X. *J. Phys. Chem. B* **2004**, *108*, 1–66699.
(36) Yan, R.; Sun, X.; Wang, X.; Peng, Q.; Li, Y. *Chem. Eur. J.* **2003**, *11*, 2183.
(37) Dosev, D.; Nichkova, M.; Liu, M.; Guo, B.; Liu, G.; Hammock, B. D.; Kennedy, I. M. *J. Biomed. Opt.* **2006**, *10*, 064006.

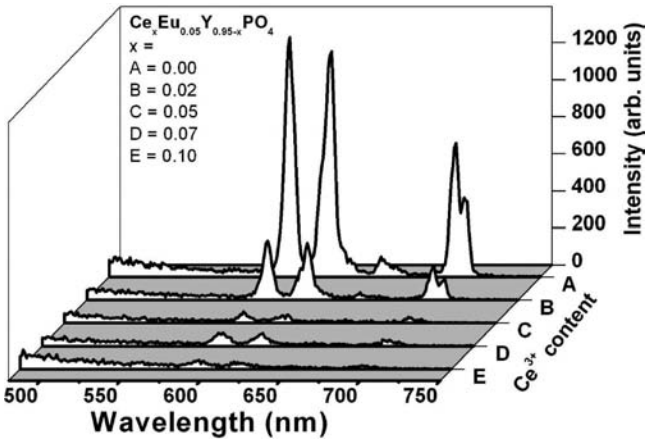

Figure 13. Emission spectra of $Ce_xEu_{0.05}Y_{0.95}PO_4$ (0.00, 0.02, 0.05, 0.07, 0.10).

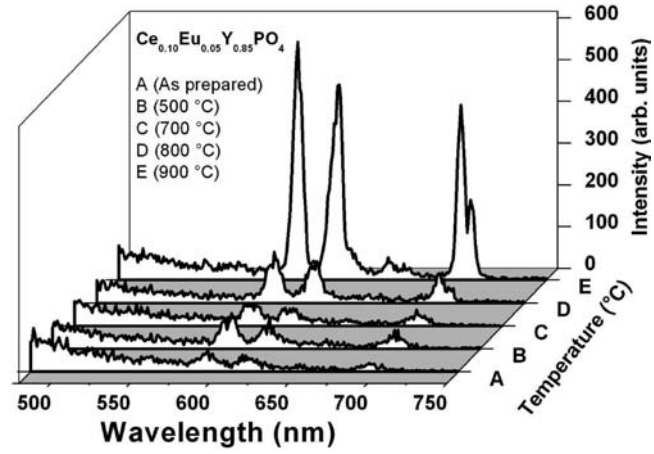

Figure 14. Emission spectra of $Ce_{0.10}Eu_{0.05}Y_{0.85}PO_4$ at different annealing temperatures.

650 nm corresponding to $^5D_0 \rightarrow {}^7F_3$ transitions is also observed. The emission spectrum when excited at a wavelength of 255 nm is weak as compared to that excited at 395 nm.

Excitation spectra of $Ce_xEu_{0.05}Y_{0.95-x}PO_4$ ($x = 0$, 0.02, 0.05, 0.07, 0.10) when emitted at 593 nm (see the Supporting Information, Figure S5) are similar to that of $Eu_{0.05}Y_{0.95}PO_4$. However, peak intensities at 255 nm (a broad peak) due to the Eu−O charge transfer band (CTB) and 395 nm (Eu^{3+}) decrease with Ce^{3+} dopants. Li and Yam[22] reported that Ce^{3+} has an absorption peak at 256 nm (4f−5d transition), which is overlapping with Eu−O CTB. These authors found that efficient luminescence of Tb^{3+} could be obtained by energy transfer from Ce^{3+} to Tb^{3+}. In order to see such an energy transfer process, we have carried out emission spectra of $Ce_xEu_{0.05}Y_{0.95-x}PO_4$ ($x = 0$, 0.02, 0.05, 0.07, 0.10) when excited at 255 nm. It is found that emission spectra (see the Supporting Information, Figure S6) are similar to that of $Eu_{0.05}Y_{0.95}PO_4$. Instead of increasing luminescence intensity, the intensity drops drastically even for 2 atom % Ce^{3+}. Thus, energy transfer from Ce^{3+} to Eu^{3+} is very poor for Ce^{3+} codoping in $Eu_{0.05}Y_{0.95}PO_4$. It is likely that even when there is energy transfer from Ce^{3+} to Eu^{3+}, most of the excited photons will be absorbed by nearby surrounding phonons of water molecules associated in the hexagonal structure. The signature of the quenching effect due to water molecules is indicated by the extent of reduction of absorption intensity of Ce^{3+} or Eu−O centered at 255 nm with increasing Ce^{3+} dopants.

Figure 13 shows the emission spectra of $Ce_xEu_{0.05}Y_{0.95-x}PO_4$ ($x = 0$, 0.02, 0.05, 0.07, 0.10) when excited at 395 nm. The luminescence intensity of Eu^{3+} decreases suddenly with increase of the Ce^{3+} codopant concentrations. Above $x = 0.02$, the luminescence intensity is almost constant. The decrease of the luminescence intensity may be due to the following possibilities: (1) a redox reaction between Ce^{3+} and Eu^{3+} to give Ce^{4+} and Eu^{2+}, (2) a distortion in structure or phase inhomogeneity such as Eu_2O_3 phase segregation from YPO_4, and (3) a quenching effect due to water molecules, etc. In order to check for the presence of Eu^{2+}, an emission spectrum was recorded in the range of 380−750 nm. No peak corresponding to Eu^{2+} emission is observed in the expected range of 380−550 nm (see the Supporting Information, Figure S6). This was supported by an XPS study, where there are no peaks corresponding to Eu^{2+} and Ce^{4+}. Thus, the first possibility is ruled out. The XRD study shows a single phase with a hexagonal structure for all Ce^{3+} codoping in $Eu_{0.05}Y_{0.95}PO_4$ samples. Also, it is established that there is an enhancement in the unit cell volume of the hexagonal phase (Table 1). The second possibility is also ruled out. From an FTIR study, it is observed that water molecules are associated in a hexagonal structure. Also, it was reported that water molecules were associated in a hexagonal/monoclinic structure.[19] Water molecules are near the activator (e.g., $Ln^{3+} = Tb$). Our prepared compounds are based on the wet-chemical synthesis route. There is an absorption of water molecules, which was confirmed by an FTIR study. Water molecules act as quenchers (discussed later). Thus, a decrease in luminescence intensity is related to the extent of content of water molecules in the hexagonal phase with an increase of Ce^{3+} dopants.

When the $Ce_{0.10}Eu_{0.05}Y_{0.85}PO_4$ sample is annealed at different temperatures (Figure 14), there is a sudden emergence of an Eu^{3+} emission peak at 900 °C which is not observed until 800 °C. As stated above in the XRD studies, there is a phase transformation to the dehydrated form from hydrated $Ce_{0.10}Eu_{0.05}Y_{0.85}PO_4$ as the temperature rises from 800 to 900 °C. The presence of OH^- ions, which are efficient quenchers of luminescence through multiphonon relaxation,[38] in the hydrated $Ce_{0.10}Eu_{0.05}Y_{0.85}PO_4$ sample heated to 800 °C results in a significant reduction of the luminescence intensity. It is noted that the origin of high luminescence intensity in the 900 °C heated sample is due to the loss of OH^- ions, which is confirmed by the crystal structure transformation from the hydrated form to the dehydrated phase.

Further, in order to compare the luminescence intensity, the integrated area under the curve of magnetic and electric dipole transitions was determined by fitting with Gaussian distribution function

$$I = I_B + \sum_{i=1}^{n} \frac{A_i}{w_i \sqrt{\pi/2}} e^{-2(\lambda - \lambda_{ci})^2/w_i^2} \qquad (2)$$

where I is the intensity, I_B is the background intensity, w_i is the width at half-maximum intensity of the curve, and A_i is the area under the curve. λ is the wavelength, and λ_{ci} is the mean wavelength value corresponding to the transition. All the fittings were carried out in the ranges of 580−605 and 605−630 nm for magnetic ($^5D_0 \rightarrow {}^7F_1$) and electric dipole ($^5D_0 \rightarrow {}^7F_2$) transitions, respectively. The relative intensity ratio of $^5D_0 \rightarrow$

(38) Blasse, G.; Grabmaier, B. C. *Luminescent Materials*; Springer Verlag: Berlin, 1994.

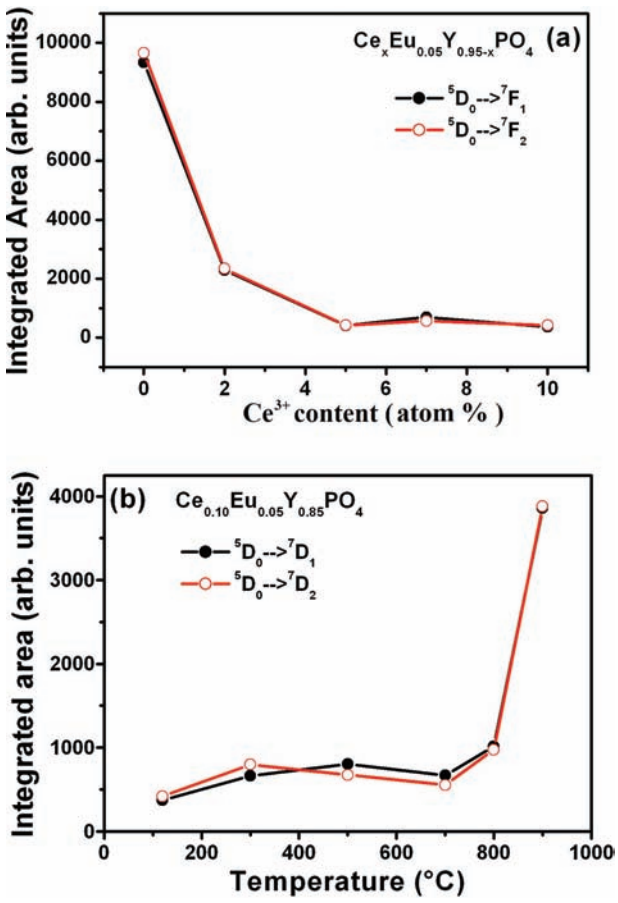

Figure 15. Integrated area of $^5D_0 \rightarrow {}^7F_1$ and $^5D_0 \rightarrow {}^7F_2$ transitions at an excitation wavelength of 395 nm at (a) different Ce^{3+} concentrations in $Ce_xEu_{0.05}Y_{0.95-x}PO_4$ and (b) different annealing temperatures in $Ce_{0.10}Eu_{0.05}Y_{0.85}PO_4$.

$^7F_2$ to $^5D_0 \rightarrow {}^7F_1$ transitions can be used as a sensitive parameter for understanding the symmetry around the Eu^{3+} in the host material. This parameter, called the asymmetric ratio (I_{AS}), is defined as

$$I_{AS} = \frac{\int_{605}^{630} I_2 \, d\lambda}{\int_{580}^{605} I_1 \, d\lambda} \tag{3}$$

where I_1 and I_2 represent the integrated intensities of $^5D_0 \rightarrow {}^7F_1$ and $^5D_0 \rightarrow {}^7F_2$ transitions of Eu^{3+}, respectively. The intensity ratio I_{AS} for $Ce_xEu_{0.05}Y_{0.95-x}PO_4$ ($x = 0.00, 0.02, 0.05, 0.07, 0.10$) and $Ce_{0.10}Eu_{0.05}Y_{0.85}PO_4$ at different annealing temperatures (300, 500, 700, 800, and 900 °C) is found to be 1.00 ± 0.2 for all the samples. This has been attributed to the equal occupancy of symmetric and asymmetric sites by Eu^{3+} ions.

Figure 15 shows the change of integrated area of $^5D_0 \rightarrow {}^7F_1$ and $^5D_0 \rightarrow {}^7F_2$ transitions with respect to Ce^{3+} concentrations and that of $Ce_{0.10}Eu_{0.05}Y_{0.85}PO_4$ at different annealing temperatures. The steep drop of luminescence intensity of Eu^{3+} is observed with an increase of Ce^{3+} concentrations up to 2 atom %, and then the luminescence intensity is almost constant above 2 atom % (Figure 15a). When the $Ce_{0.10}Eu_{0.05}Y_{0.85}PO_4$ sample is annealed at higher temperature, the luminescence intensity of Eu^{3+} shows a sharp increase at 900 °C (Figure 15b), which is due to the loss of the OH^- group on conversion to the dehydrated tetragonal phase from the hydrated hexagonal phase.

Zollfrank et al.[25] reported a similar result in hydrated europium(III) orthophosphate, $EuPO_4 \cdot nH_2O$, in which the intensity ratio of the magnetic dipole $^5D_0 \rightarrow {}^7F_1$ transition to the electric dipole $^5D_0 \rightarrow {}^7F_2$ transition decreased with increasing calcination temperature up to 600 °C, clearly indicating the presence of the hypersensitive, forced electrical dipole $^5D_0 \rightarrow {}^7F_2$ due to a lack of inversion symmetry. They further explained that the loss of water during heating up to 600 °C is responsible for the variation in the emission characteristics of $EuPO_4 \cdot nH_2O$.

Water molecules in the samples act as primary centers of nonradiative transition. The rate of the nonradiative transition, R_0, is exponential and can be expressed as

$$R_0 = ae^{-(\Delta E - 2h\nu_{max})b} \tag{4}$$

where a and b are constants. ΔE is the difference in energy between the excited and ground states of the Eu^{3+} ion. ν_{max} is the highest available vibrational modes of the surroundings of the rare-earth ion. In the Eu^{3+} ion, ΔE is about 10 000−15 000 cm^{-1} and the value is comparable with the third overtone stretching vibration of the OH group (3500 cm^{-1}). This OH functional group arises from water molecules absorbed or associated with a hexagonal structure. Now, the R_0 value becomes large, since $\Delta E \approx 2h\nu_{max}$. This results in a significant extent of nonradiative transfer of energy from the excited state of the Eu^{3+} ion to the different vibration modes of OH species, leading to a reduction in Eu^{3+} luminescence intensity. In the excited state of Eu^{3+}, the process of excited photon loss due to transfer of energy to the nearby surrounding phonons of OH group is termed as multiphonon relaxation. The rate of excited photon/energy loss is very fast ($>10^{+10}$ per second), and therefore it is associated with a nonradiative process.[38,39]

2.7.2. Lifetime Study. Figure 16a shows the luminescence decay for the $^5D_0$ level of Eu^{3+} in $Ce_xEu_{0.05}Y_{0.95-x}PO_4$ ($x = 0.00$, 0.02, 0.05, 0.07, 0.10). The excitation wavelength was fixed at 395 nm.

To understand the behavior of luminescence decay, we have tried fitting (using the Origin 6.1 program) to the decay data. It is found that curves follow the monoexponential decay

$$I_t = I_0 e^{-t/\tau}$$

where I_t is the intensity at time t, I_0 is the intensity at $t = 0$, and τ is the decay lifetime. With increasing Ce^{3+} codopant concentrations, the lifetime for the $^5D_0$ level of Eu^{3+} decreases from 2.1 to 0.5 ms, as shown in Table 4.

When the $Ce_{0.10}Eu_{0.05}Y_{0.85}PO_4$ sample is annealed at different temperatures (Figure 16b), the lifetime value shows little change up to 800 °C. However, the decay time of the 900 °C heated sample, in which the phase transformation occurs, shows a significant enhancement in decay lifetime (Table 4). This sudden increase in decay lifetime is related to the phase transformation from a hydrated hexagonal phase to a dehydrated tetragonal phase as well as the loss of the OH^- ions.

2.8. Effect of D_2O Solvent on Luminescence. In order to check the effect of OH on the luminescence of the sample, we have prepared $Ce_{0.02}Eu_{0.05}Y_{0.93}PO_4$ in D_2O solvent under an argon atmosphere. Stoichoimetric amounts of the reactants ($Ce_2(CO_3)_3 \cdot xH_2O$, Eu_2O_3, $Y_2(CO_3)_3 \cdot xH_2O$) were dissolved in the minimum amount of concentrated HCl, and the excess HCl was removed by evaporation with addition of D_2O. The resulting

(39) Layne, C. B.; Lowdermilk, W. H.; Weber, M. J. *Phys. Rev. B* **1977**, *16*, 10.

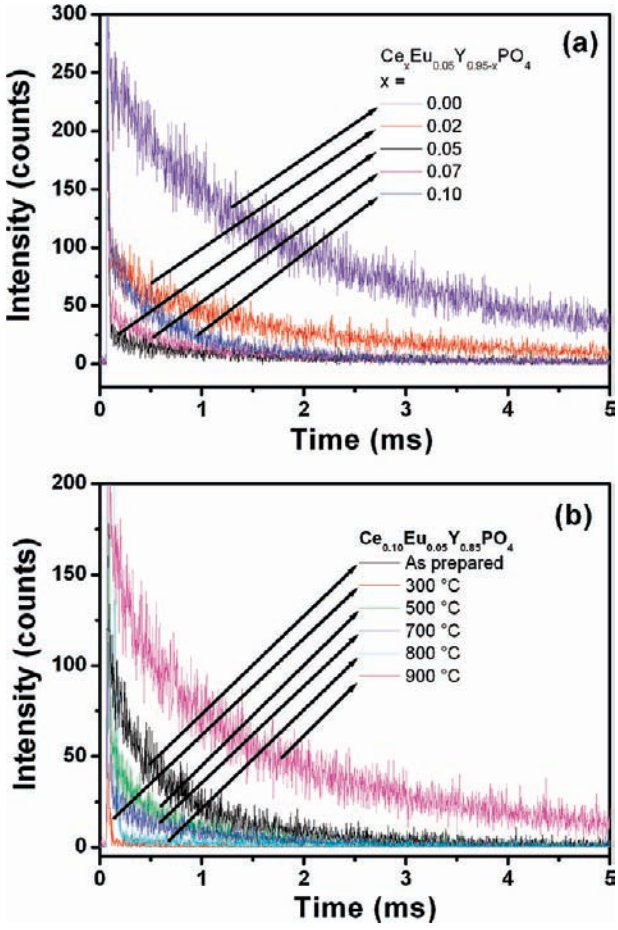

Figure 16. Decay curves for the $^5D_0$ level of Eu^{3+} in (a) $Ce_xEu_{0.05}Y_{0.95-x}PO_4$ ($x = 0.00, 0.02, 0.05, 0.07, 0.10$) and (b) $Ce_{0.10}Eu_{0.05}Y_{0.85}PO4$ at different annealing temperatures.

Table 4. Lifetime Values for the $^5D_0$ Level of Eu^{3+} (Monoexponential Fitting) in $Ce_xEu_{0.05}Y_{0.95-x}PO_4$ at Different Ce^{3+} Concentrations and $Ce_{0.10}Eu_{0.05}Y_{0.85}PO_4$ at Different Annealing Temperatures

sample no.	sample	lifetime (ms)
1	$Eu_{0.05}Y_{0.95}PO_4$, as prepared	2.07 ± 0.01
2	$Ce_{0.02}Eu_{0.05}Y_{0.93}PO_4$, as prepared	1.44 ± 0.02
3	$Ce_{0.05}Eu_{0.05}Y_{0.90}PO_4$, as prepared	0.70 ± 0.05
4	$Ce_{0.07}Eu_{0.05}Y_{0.88}PO_4$, as prepared	0.55 ± 0.02
5	$Ce_{0.10}Eu_{0.05}Y_{0.85}PO_4$, as prepared	0.51 ± 0.01
6	$Ce_{0.10}Eu_{0.05}Y_{0.85}PO_4$, 300 °C	
7	$Ce_{0.10}Eu_{0.05}Y_{0.85}PO_4$, 500 °C	0.37 ± 0.02
8	$Ce_{0.10}Eu_{0.05}Y_{0.85}PO_4$, 700 °C	0.42 ± 0.03
9	$Ce_{0.10}Eu_{0.05}Y_{0.85}PO_4$, 800 °C	
10	$Ce_{0.10}Eu_{0.05}Y_{0.85}PO_4$, 900 °C	1.41 ± 0.01

solution was heated at 80 °C for 30 min under an argon atmosphere, and a stoichoimetric amount of $(NH_4)H_2PO_4$ was added. The solution was refluxed at 120 °C for 2 h in D_2O medium.

From the PL studies (Figure 17), the emission intensity of $Ce_{0.02}Eu_{0.05}Y_{0.93}PO_4$ prepared in D_2O solvent shows about a 2-fold increase as compared to that prepared in H_2O solvent when excited at 395 nm. The possible reason for the increase in luminescene might be due to the substitution of the luminescence quencher OH by OD. The stretching vibration of OD is about 2500 cm^{-1}, which is less than that of OH (3450 cm^{-1}). Figure 18 shows the IR data of $Ce_{0.02}Eu_{0.05}Y_{0.93}PO_4$ prepared with D_2O and H_2O solvents. Only the data range

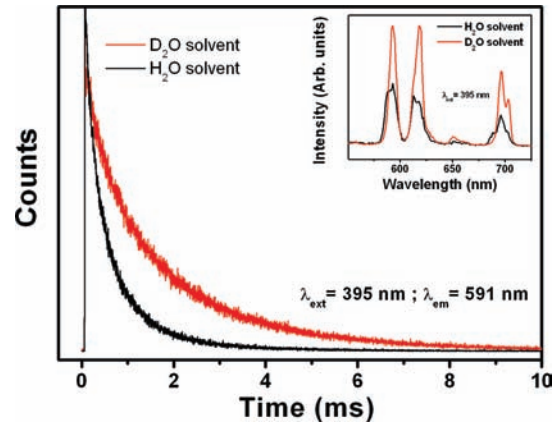

Figure 17. Decay curves for the $^5D_0$ level of Eu^{3+} in $Ce_{0.02}Eu_{0.05}Y_{0.93}PO_4$ in different solvents. The inset shows the luminescence spectra of $Ce_{0.02}Eu_{0.05}Y_{0.93}PO_4$ in different solvents.

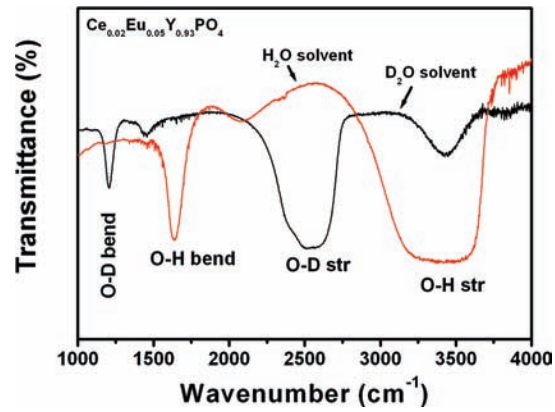

Figure 18. Infrared spectra of $Ce_{0.02}Eu_{0.05}Y_{0.93}PO_4$ prepared in different solvents.

1000−4000 cm^{-1} is shown in order to see their vibration absorptions. Multiphonon relaxation is significantly reduced when the OH vibration is replaced by OD. The enhancement in luminescence is due to the extent of decrease of multiphonon relaxation. Luminescence decay lifetimes for the $^5D_0$ level of Eu^{3+} in $Ce_{0.02}Eu_{0.05}Y_{0.93}PO_4$ are 0.58 and 1.68 ms, respectively, when the solvent changes from H_2O to D_2O (inset of Figure 17). Duplicate experiments were carried out, and similar results were obtained.

It should be noted that an enhancement of luminescence was obtained from a highly Ce^{3+} doped sample ($Ce_{0.10}Eu_{0.05}Y_{0.85}PO_4$) when the solvent changes from H_2O to D_2O. This confirms that a decrease in luminescence on doping with Ce^{3+} is due to the absorption of H_2O molecules, which are near the luminescence activator (Eu^{3+}).

3. Conclusions

Ce^{3+}-codoped YPO_4:Eu^{3+} has been prepared by the polyethylene glycol−glycerol route. Addition of Ce^{3+} ions to YPO_4:Eu^{3+} leads to a sharp decrease in the luminescence intensity of Eu^{3+}. XRD analysis clearly shows the phase transformation from a tetragonal to a hydrated hexagonal phase. A TEM study shows the change of shape morphology from uniform to distorted nanorods as the heat treatment temperature increases up to 900 °C. The decrease in the luminescent intensity of Eu^{3+} is due to the presence of OH^- ion, which is an efficient luminescence quencher through multiphonon relaxation. The luminescence

intensity can be recovered by annealing the Ce^{3+}-codoped YPO_4:Eu^{3+} at 900 °C. This has been attributed to a phase transformation of the hydrated hexagonal to the dehydrated tetragonal phase. XPS studies further confirm that the change in the luminescence intensity of Eu^{3+} is mainly due to the water molecule present in the sample and not because of the possible charge conversion between Eu^{3+} and Ce^{3+}. In the presence of D_2O solvent as the reaction medium, the luminescence intensity increases significantly.

4. Experimental Section

4.1. Reagents and Materials. Yttrium(III) carbonate hydrate ($Y_2(CO_3)_3 \cdot xH_2O$, 99.9%), cerium carbonate hydrate ($Ce_2(CO_3)_3 \cdot xH_2O$, 99.9%) and ammonium dihydrogen phosphate ($NH_4H_2PO_4$, 99.999%), all from Sigma-Aldrich, europium(III) oxide (Eu_2O_3, 99.9%) from Alfa Aesar, polyethylene glycol (PEG) 1000 from Fluka, and glycerol, methanol, and hydrochloric acid were used as received without further purification. Double-distilled water was used throughout the experiment.

4.2. Synthesis of Eu- and Ce-Doped YPO_4. Pure YPO_4, $Eu_{0.05}Y_{0.95}PO_4$, $Ce_{0.05}Y_{0.95}PO_4$, and $Ce_xEu_{0.05}Y_{0.95-x}PO_4$ ($x = 0.02$, 0.05, 0.07, 0.10) nanoparticles were synthesized by the polyethylene glycol−glycerol route. In a typical synthesis procedure of $Ce_xEu_{0.05}Y_{0.95}PO_4$ ($x = 0.02$), 0.02 g of $Ce_2(CO_3)_3 \cdot xH_2O$, 0.038 g of Eu_2O_3, and 0.723 g of $Y_2(CO_3)_3 \cdot xH_2O$ were dissolved in concentrated HCl and excess acid was removed by evaporation with addition of water. The resulting transparent solution was mixed with 10 g of PEG-1000 and 50 mL of glycerol and heated in a round-bottom flask at 80 °C for 30 min. $(NH_4)H_2PO_4$ (0.5 g) was added to the above solution, and the solution was refluxed at 120 °C for 2 h. The resulting white precipitate was collected by centrifugation at 10 000 rpm after washing with methanol.

The chemical equation for the formation of $LnPO_4$ (Ln = Y, Eu, Ce) is

$$Ln^{3+} + Cl^- + (NH_4)H_2PO_4 + xH_2O \rightarrow LnPO_4 \cdot xH_2O \downarrow + NH_4Cl + H_3PO_4 \quad x = 0-3$$

In order to see the phase change, the as-prepared sample of $Ce_{0.10}Eu_{0.05}Y_{0.85}PO_4$ was annealed at different temperatures (300, 500, 700, 800, and 900 °C) for 12 h each.

4.3. Characterization of the Nanoparticles. A Philips X-ray diffractometer (PW 1071) with Cu Kα (1.5405 Å) radiation and a Ni filter was used for the X-ray diffraction (XRD) study. In situ high-temperature XRD studies were carried out on a Philips X'PERT model using platinum as the sample holder. All patterns were recorded over the angular range $10 \leq 2\theta/\text{deg} \leq 70$ with a step size of $\Delta 2\theta = 0.02$. The average crystallite size (t) was calculated using the Debye−Scherrer relation $t = 0.9\lambda/\beta \cos \theta$, where λ is the wavelength of the X-radiation and β is the full width at half-maximum (fwhm). The powder samples were ground and dispersed in methanol on a glass slide and allowed to dry.

Thermal analyses of as-prepared powder samples were carried out using a thermogravimetic−differential thermal analysis (TG-DTA) instrument (SETARAM 92-16.18). The samples under examination were heated at a rate of 5 °C min^{-1} under an ambient atmosphere.

A TG-DTA instrument (Setaram Setsys Evolution) coupled with a quadrupole mass spectrometer (QMS 422) was used for thermogravimetric mass spectrometry analysis under a pure oxygen atmosphere at a rate of 8 mL per minute with a heating rate of 5 °C min^{-1}.

For the characterization of the nanoparticles, IR spectra were recorded on a FT-IR spectrometer (Bomem MB 102). Powder samples were studied by making thin pellets with KBr.

A CM-200 transmission electron microscope was used for recording TEM images. For the TEM measurement, the powder samples were ground and dispersed in methanol. A drop of the dispersed particles was placed over the carbon-coated copper grid and evaporated to dryness at room temperature.

X-ray photoelectron spectroscopy (XPS) studies were conducted in a UHV chamber (base pressure $<2 \times 10^{-8}$ mbar) using a VG CLAM-2 analyzer with a nonmonochromatic twin Mg X-ray ($h\nu$ = 1253.6 eV) source. The analyzer was operated in the CAE (constant analyzer energy) or high-energy resolution mode. Under these conditions, energy resolutions and chemical shifts could be detected to about ±0.5 eV. All binding energies were referenced to the C1s peak at 284.6 eV of the surface adventitious carbon.

The surface area measurements were carried out on a Quantachrome Autosorb-1 instrument. The samples were dehydrated under vacuum at 255 °C for 4 h prior to an analysis. The physical adsorption and desorption isotherms were recorded at 77 K. N_2 gas was used as the carrier gas.

All the luminescence spectra were recorded using an Edinburgh FLS920 instrument equipped with a 450 W xenon lamp. Decay lifetimes were recorded using a microsecond flashlamp (100 W). Powder samples were dispersed in methanol, and the dispersions were spread over the quartz slide and dried at room temperature.

Acknowledgment. We thank Dr. T. Mukherjee (Chemistry Group, BARC) and Dr. D. Das (Chemistry Division, BARC) for their support and encouragement during this work. M.N.L. thanks the University Grant Commission, New Delhi, India, for providing a UGC Research Fellowship in Science for Meritorious Students.

Supporting Information Available: Figures giving thermogravimetric analysis (TGA) and differential thermal analysis (DTA) data for $Ce_{0.10}Eu_{0.05}Y_{0.85}PO_4$ nanorods, XPS spectra of 900 °C heated $Ce_{0.02}Eu_{0.05}Y_{0.93}PO_4$ along with as-prepared and 900 °C heated $Ce_{0.10}Eu_{0.05}Y_{0.85}PO_4$, and excitation and emission spectra of $Ce_xEu_{0.05}Y_{0.95}PO_4$ (0, 0.02, 0.05, 0.07, and 0.10). This material is available free of charge via the Internet at http://pubs.acs.org.

JA909578S